Available online at www.sciencedirect.com
SCIENCE DIRECT®
Journal of Catalysis 236 (2005) 346–355
JOURNAL OF CATALYSIS
www.elsevier.com/locate/jcat

The reactions of cyclohexene on Au(111)-supported molybdenum carbide nanoparticles

Denis V. Potapenko [a], Jillian M. Horn [a,b], Michael G. White [a,b,*]

[a] *Chemistry Department, Brookhaven National Laboratory, Upton, NY 11973, USA*
[b] *Department of Chemistry, SUNY Stony Brook, Stony Brook, NY 11794, USA*

Received 27 June 2005; revised 23 September 2005; accepted 28 September 2005

Available online 10 November 2005

Abstract

The reactivity of cyclohexene on Au(111)-supported molybdenum carbide nanoparticles was studied using temperature-programmed desorption (TPD) and Auger electron spectroscopy (AES) techniques. The surfaces were prepared by reactive layer-assisted deposition (RLAD), in which Mo metal is deposited onto ethylene adsorbed on a Au(111) surface, followed by annealing to 700 K. We have shown that gold encapsulates the MoC_x nanoparticles to some extent on annealing. This encapsulation can be removed by ion sputtering at room temperature. Although the sputtered MoC_x/Au(111) surface was very reactive toward adsorbed cyclohexene, the selectivity for partial dehydrogenation to benzene was very poor (0.06), with most of the reacting cyclohexene decomposing to surface carbon and molecular hydrogen. In contrast, the Au-encapsulated MoC_x nanoparticles exhibit low total activity, but very high (>0.95) selectivity for partial dehydrogenation to benzene, with no detectable decomposition to surface carbon. The low overall reactivity and high selectivity of Au-encapsulated MoC_x surfaces for partial cyclohexene dehydrogenation are explained by gold selectively blocking high reactivity sites on the MoC_x clusters.

Keywords: Reactive deposition; Molybdenum carbide; Nanoparticle; Au(111); Encapsulation; Cyclohexene; Dehydrogenation

1. Introduction

It has been documented that the early transition metal carbides have catalytic properties similar to the Pt group metals [1–3]. In addition to being less costly, the transition metal carbides can have additional advantages in terms of resistance to poisoning and selectivity for certain reactions. One of the more widely studied systems is molybdenum carbide, which has been shown to be an active catalyst in a wide variety of reactions, including hydrocarbon conversion [2–10], ammonia synthesis [11], hydrodesulfurization and hydrodenitrogenation [12,13], and the water–gas shift reaction [14,15]. Chen and coworkers have compared the reactivity of carbon-modified Mo(110) to Pt(111) surfaces for the selective dehydrogenation of cyclohexene, a prototypical dehydrogenation reaction catalyzed by the noble metals [3,16,17]. Although the activity per metal atom is lower for C/Mo(110) than Pt(111), the selectivity toward benzene production as a gas-phase product is significantly higher [17,18]. By comparison, the Mo(110) pure metallic surface exhibits high activity but very poor selectivity, with the dominant reaction being complete decomposition of cyclohexene to surface carbon and molecular hydrogen.

Whereas carburization of the pure metal surface leads to dramatic changes in reactivity, further optimization may be attainable by changing the surface structure and relative carbon/metal composition. Indeed, molybdenum carbide has a complex phase diagram with bulk forms with varying Mo/C ratios and different crystal structures [19]. These include the stable β-Mo_2C (hexagonal close packed) phase and several nonstoichiometric, high-temperature MoC_{1-x} phases with both hexagonal and cubic structures. Surfaces of the carbide can also be carbon- or metal-terminated, and nonstoichiometric Mo/C ratios are often observed on carburized Mo surfaces. The reactivity has also been found to depend strongly on the atomic composition and structure (surface and bulk), which in turn can be further modified by thermal treatment [8,11,20,21]. For example,

* Corresponding author. Fax: +1 631 344 5815.
E-mail address: mgwhite@bnl.gov (M.G. White).

0021-9517/$ – see front matter
doi:10.1016/j.jcat.2005.09.029

a molybdenum carbide surface annealed to high temperatures (>1000 K) with mostly subsurface (interstitial) carbon is active toward dissociation of ethylene and cyclopentene, whereas molybdenum carbide-containing surface carbon is inert to these two compounds [21].

Another approach to modifying the surface structure and chemical activity of materials involves their dispersion as particles to yield high surface area catalysts. In general, size effects and support interactions influence the electronic and atomic structure of metallic particles and can lead to significant changes in activity relative to the bulk material [22]. For molybdenum carbide, temperature-programmed reaction (TPR) [2,15,23] and sonochemical methods [10,24] have been used to prepare unsupported carbide catalysts in various crystal phases (β-Mo_2C (hcp), α-MoC_{1-x} (fcc), Mo_2C (fcc)), with the smallest particle sizes lying in the 2–7 nm range depending on the preparation method. TPR has also been used to prepare carbides on various supports, including Al_2O_3, SiO_2, and ZSM-5 zeolite [4,6,7,13,25,26]. In general, the catalytic activities of the dispersed catalysts are found to depend on the carbide phase [5,8,11] and are strongly influenced by the support material [4,6,25]. For example, the conversion of CH_4 over unsupported catalysts (β-Mo_2C, α-MoC_{1-x}) yields primarily hydrogen, ethane, and ethylene, whereas conversion over the supported Mo_2C/ZSM-5 catalyst results in benzene formation with very high selectivity (∼70%) [6,7,25]. Although such experiments suggest the possibility of tailoring the catalytic activity of the dispersed carbides for specific reactions, key questions remain concerning the nature of the surface active sites and how they are influenced by the particle size and structure (bulk and surface), surface chemical composition, and support interactions.

In this work we present a reactivity study of molybdenum carbide nanoparticles prepared on a Au(111) substrate that addresses a number of the important issues noted above: surface chemical composition, thermal stability, and modification of surface active sites. In this way, the present study is a step toward bridging the gap between surface science studies on extended (flat) surfaces and high-surface area carbide catalysts. The molybdenum carbide nanoparticles were prepared on the Au(111) using reactive layer assisted deposition (RLAD), as recently detailed in a previous study [27]. The Au(111) substrate was chosen for its ability to act as a nucleation template for metallic nanoparticles and is sufficiently inert so as not to induce other surface reactions. In the RLAD method, molybdenum carbide nanoparticles are formed by the reaction of Mo metal atoms deposited by physical vapor deposition (PVD) onto a reactive layer of ethylene that is physisorbed on the Au(111) substrate at low temperature (<100 K). This procedure results in the formation of small MoC_x particles (∼1.5 nm), with a temperature-averaged Mo/C ratio of 1.2 ± 0.2 [27]. Auger spectroscopy shows that the surface composition is strongly dependent on annealing temperature with both carbon diffusion and Au atom migration occurring at elevated temperatures. The latter is similar to Au encapsulation of Mo metal nanoparticles deposited on a Au(111) substrate, as was recently demonstrated in this laboratory [28].

Chemical reactivity studies presented here focus on the dehydrogenation reactions of cyclohexene, which are prototypical of hydrocarbon conversion reactions catalyzed by the metal carbides [2–10]. The reactivity and product distributions are found to be sensitive to the surface chemical composition of the MoC_x particles, which were modified by thermal treatment and sputtering of the topmost layers. The surface reactivity and chemical composition were determined by a combination of temperature-programmed desorption (TPD) and Auger electron spectroscopy (AES). The results of these measurements are used to extract quantitative branching ratios for the observed reactions and are compared with similar data from single-crystal surfaces of pure metals (i.e., Pt(111) and Mo(110)) and carburized metals (C/Mo(110)). A key finding is that diffusion of Au atoms onto the MoC_x nanoparticles during high-temperature annealing dramatically changes their surface reactivity. The later is attributed to Au atoms blocking highly active sites that promote C–C bond breaking and results in surfaces that exhibit much higher selectivity for conversion of cyclohexene to benzene.

2. Experimental methods

All experiments presented in this paper were performed in an ultra-high-vacuum (UHV) chamber with a typical background pressure of 2×10^{-10} Torr. The chamber was equipped with quadrupole mass spectrometer (Hiden Analytical), Auger spectrometer (Physical Electronics), a metal evaporation source (Oxford Applied Research), an atomic hydrogen source (Oxford), and a sputter gun (LK Technologies). A disk-shaped Au(111) single crystal (10 mm diameter) was mounted on a liquid N_2 cooled manipulator with two Ta wires that were also used for resistive heating. The sample temperature was measured by a K-type thermocouple in direct contact with the gold. The Au(111) surface was cleaned by cycles of sputtering with Ne^+ (1 keV), followed by annealing at 850 K. The surface was determined to be clean with AES. Mo was deposited on the sample by PVD using the e-beam evaporator. Deposition rates of the evaporator were calibrated with a quartz microbalance. All of the substances (ethylene, cyclohexene, benzene, and cyclohexane) were deposited on the sample through a directed doser. Atomic deuterium was deposited using a thermal cracker, whereby D_2 was passed through an e-beam heated ThO_2-coated metal capillary directed at the sample. All TPD experiments were performed with 2 K/s heating rate. A linear temperature ramp was provided by an electronic process control unit (Eurotherm). A shielded quadrupole mass spectrometer monitored up to 10 ionic masses simultaneously.

Atomic surface concentrations of elements were calculated from peak-to-peak heights of Au (74 eV), Mo (190 eV), C (275 eV), and O (510 eV) features in the AES spectra, assuming that these were the only elements present at the surface. Unless stated otherwise, standard formula and AES sensitivity coefficients were used [29]. During the preparation of MoC nanoparticles, oxygen contamination due to background water in the chamber could not be avoided. Typical oxygen content of the MoC/Au surfaces was 5%, and a typical carbon content was

30% (i.e., an O/C ratio of 1:6). It has been shown that oxygen modification of the C/Mo(110) surface does not cause qualitative changes in the surface reactivity with cyclohexene when the O/C ratio does not exceed 1:4 [30].

Liquid compounds (cyclohexene, benzene, and cyclohexane) were held in glass containers and degassed by multiple freeze–thaw cycles before use. Deuterium-substituted benzene, cyclohexene, and cyclohexane (Sigma–Aldrich) were used to improve the signal-to-noise ratio for molecular hydrogen detection. The sample vapor of interest was introduced into a small, backing volume at low pressure (typically, 100 mTorr) located behind a UHV shutoff valve with limited conductance. A capacitance manometer (MKS) was used to measure the sample pressure in the backing volume to an accuracy of ±1 mTorr. Dosing was accomplished by opening the shutoff valve to allow the vapor to leak into the stainless steel dosing tube for a prescribed period of time. The exit of the dosing tube had a diameter similar to that of the crystal (∼10 mm) and could be positioned <1 mm from the surface. Experiments confirmed that deposition rates were consistent and had a linear dependence on the pressure of the gas in the backing volume.

For analysis of the TPD data, the relative sensitivity of the mass spectrometer for different masses was needed to quantify the yields of different desorption products. Three TPD experiments were performed with deuterated benzene, cyclohexene, and cyclohexane, in which the Au(111) surface was exposed to each gas at 84 K under identical conditions (e.g., identical pressure in the backing volume and exposure time). The conditions used resulted in coverages somewhat greater than a monolayer for each compound to ensure saturation of the first layer. The parent mass for each molecule was used in these TPD measurements: $m/e = 84$ for C_6D_6, $m/e = 92$ for C_6D_{10}, and $m/e = 96$ for C_6D_{12}. For each run, the areas for the single (mono)layer and the total (single layer plus multilayer) TPD peaks were calculated. The single layer and total TPD peak areas were used to calculate sensitivity coefficients independently, assuming that the sticking was the same for each molecule. This assumption is reasonable, because the Au(111) substrate was kept at least 50 K below the respective multilayer desorption temperatures. The experimental observations that each of the C_6 molecules binds to the Au(111) surface in a "flat" configuration [31,32] and that the molecules are of nearly equal size suggest that equal numbers of molecules will be adsorbed in the first layer. Complications could arise if the doser design resulted in variations in the deposition rate for the different gases (at otherwise identical conditions), such as differences in viscosity of the different substances [33]. Dynamic viscosities at the zero density limit (appropriate for 100 mTorr) of benzene and cyclohexene extrapolated to 300 K can be found in the literature as 7.74 and 6.93 μPa s, respectively [34], and would result in only an 11% difference in deposition rates.

The calculated relative sensitivities using both sets of TPD data differed by only 10%, which is considered a measure of their uncertainties. Sensitivity factors averaged over both methods were used for the quantitative analyses discussed below. These are 0.093 for d_{10}-cyclohexene at $m/e = 92$ and 0.48 for d_{12}-cyclohexane at $m/e = 96$, taking the sensitivity of the mass spectrometer for d_6-benzene at $m/e = 84$ as 1.00. It is further assumed that the sensitivities for all deuterium substitutions of benzene are equal at the m/e of the parent molecule. Finally, the relative sensitivity for D_2 was extracted from a series of TPD experiments with d_{10}-cyclohexene on MoC/Au surface. Both the benzene and D_2 TPD peaks in these experiments originate from cyclohexene through a reaction with known stoichiometry (see the discussion of Fig. 3 below). Thus we could relate the sensitivities for C_6D_6 at $m/e = 84$, taken as 1, and D_2 at $m/e = 4$, which was found to be equal 1.3.

3. Surface characterization

Nanoparticles of MoC_x on the Au(111) surface were prepared using the RLAD technique as described in an earlier study [27]. In that work, Mo coverages of <1 ML were used for the preparation of MoC/Au surfaces with a monolayer of ethylene used as a source of carbon. Higher ethylene coverages were not achievable, because the sample holder could not be cooled to 79 K, at which temperature ethylene multilayers are stable [35]. The present study is based primarily on TPD measurements, for which reasonably high yields of surface reaction products were needed. For this reason, higher Mo coverages (about 1.5 ML) were used along with a modified RLAD procedure to provide sufficient carbon concentrations. This procedure involves the deposition of three layers of C_2H_4 (1 ML each) alternating with two layers of Mo (about 0.7 ML each). Surfaces prepared by this deposition method provided higher benzene production yields compared with the other methods tried, including those using butadiene and cyclohexene multilayers as the carbon source. (It should be noted, however, that optimization of the surface reactivity was not the aim of the present work.)

Molybdenum carbide nanoparticles on the Au(111) surface comprise a rather complex system. Previously, XPS and STM were used to investigate the composition and morphology of MoC_x nanoparticles on a Au(111) substrate [27]. In the present work, AES was used to analyze the thermal evolution of fresh MoC/Au surfaces prepared by the deposition of alternating layers of ethylene and Mo, as well as MoC/Au surfaces that were sputtered at 200 K to remove about one atomic layer. (Note that here the Au(111) surfaces with molybdenum carbide nanoparticles are referred to as "MoC/Au" for simplicity, without implying exact 1:1 stoichiometry.)

Figs. 1a and 1b show Mo/Au and C/Au atomic ratios calculated from AES spectra for the Mo/C_2H_2 layers on Au and sputtered MoC/Au surfaces that have been annealed for 1 min to progressively higher temperatures. For both surfaces, the ratios decrease for temperatures above 400 K. The Mo/Au and C/Au ratios fall from about 10 to 1 during the process of MoC cluster formation from a C_2H_4 + Mo overlayer. This dramatic decrease of the atomic ratios can be explained by the fact that ethylene and Mo form a continuous film during deposition that screens the Au AES signal (apparent surface concentration of Au at 100 K was 5%). At temperatures above 400 K, Mo and C atoms migrate on the surface to form 3-dimensional particles as reported previously [27], exposing areas of bare Au. The ap-

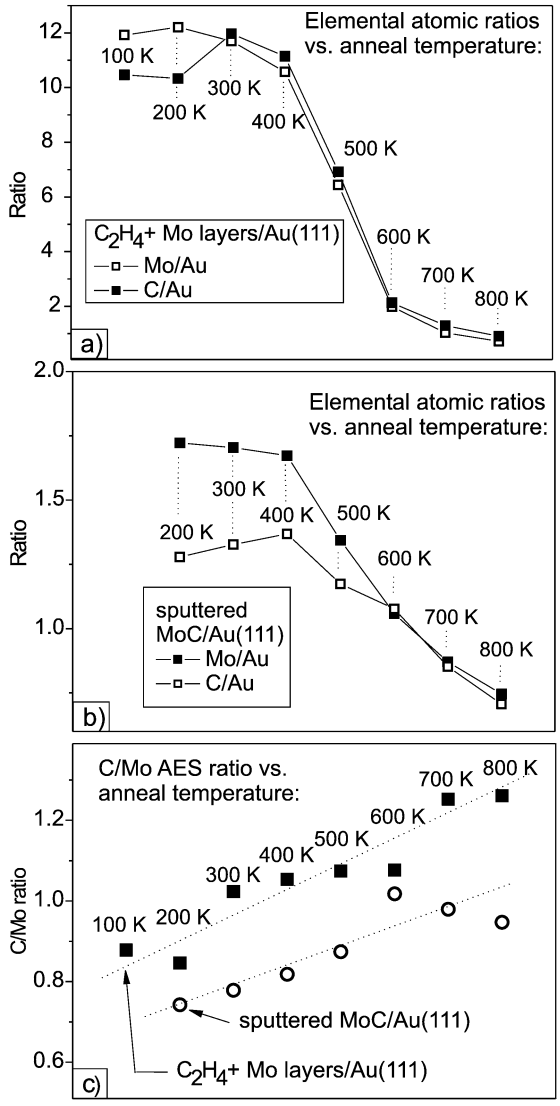

Fig. 1. (a) and (b) Mo(190 eV)/Au(74 eV) (open symbols) and C(275 eV)/Au(74 eV) (filled symbols) AES peak height ratios as a function of anneal temperature. (a) Multilayer Mo + C_2H_4 surface prepared at 90 K. (b) MoC/Au surface sputtered at 200 K. (c) C(275 eV)/Mo(190 K) AES peak height ratios as a function of anneal temperature of a multilayer Mo + C_2H_4 surface (filled symbols), and of sputtered MoC/Au surface (open symbols).

parent Au surface concentration rises to about 30%, and the Mo/Au and C/Au ratios fall to about 1.

For the sputtered MoC/Au surface, the Mo/Au and C/Au ratios decrease by a smaller factor (∼2×) with annealing to high temperature (Fig. 1b). Experiments also show that the Mo/Au and C/Au ratios increase by a similar factor when an annealed surface is sputtered to remove approximately one atomic layer. We attribute these observations to the diffusion of gold atoms onto the surfaces of the MoC nanoparticles. As discussed below, this hypothesis is supported by the observation that the reactivity of a sputtered MoC/Au surface is very different before annealing and after annealing. Similar behavior was reported in an earlier study of Mo nanoparticles deposited onto a Au(111) surface [28]. Annealing of the Mo/Au(111) surface resulted in gold encapsulation of the Mo particles that was verified by AES

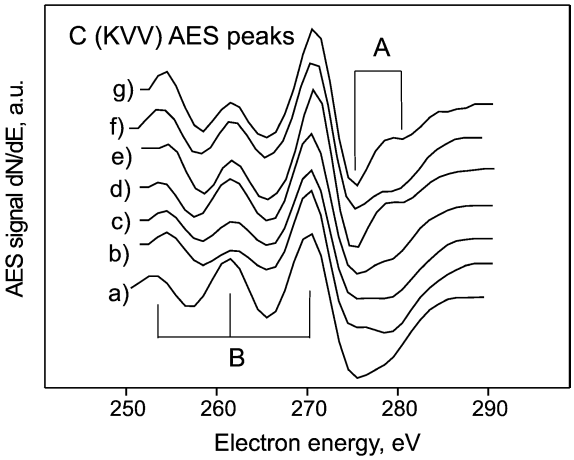

Fig. 2. AES differential spectra in the C KLL peak region. The spectra taken from: (a) Mo_2C reference sample; (b), (c), (d), and (e) Mo + C_2H_4/Au surface as prepared at 100 K and annealed to 200, 400, and 800 K, respectively; (f) MoC/Au surface sputtered at 200 K and (g) annealed to 800 K.

atomic ratios and STM studies [28]. (In this work, the term "encapsulation" is used to describe the addition of gold atoms onto the MoC particle surfaces without implying the extent of the Au coverage, for which we currently have no definitive measure.)

Analysis of the C/Mo atomic ratio in Fig. 1c reveals a more subtle aspect of the thermal evolution of the MoC/Au surfaces. In both a freshly prepared C_2H_4 + Mo overlayer and a sputtered MoC/Au surface, the C/Mo atomic ratio increases with increasing annealing temperature. Two explanations for this phenomenon are possible. First, encapsulation by Au atoms may selectively occupy Mo sites (or Mo-rich sites) and screen the Mo AES signal. Second, the carbon concentration in the MoC nanoparticles may exceed its equilibrium value, causing carbon precipitation on the surface of the nanoparticles. Both processes have some experimental justification. We have shown that gold spontaneously encapsulates Mo nanoparticles at temperatures above 300 K [28]. On the other hand, carbon encapsulation of gold particles has been observed in arc discharge [36] and SEM [37] experiments. These observations suggest the following order of increasing surface energies of the elements: C(graphite) < Au < Mo. This order is consistent with selective occupation of Mo sites by gold atoms.

The carbon concentration of the MoC_x nanoparticles can be estimated from AES spectra using the C KLL to Mo MNN peak ratio, which is about 0.5 for an annealed MoC/Au(111) surface. For this surface, a C/Mo atomic ratio is calculated as 1.1:1 using standard AES sensitivity coefficients [29] or as 1.6:1 using sensitivity coefficients taken from a separate calibration measurement using a known Mo_2C sample. According to the Mo–C phase diagram, the highest achievable concentration of carbon in a stable compound corresponds to a ratio of 1:1 [38]. Hence the excess carbon indicated by the AES measurements is likely to be present as a precipitate on the exterior of the MoC nanoparticles.

Analysis of the carbon KLL Auger line shapes also supports the carbon precipitation hypothesis. Such analyses are often used in the literature to deduce the chemical state of carbon [39–41]. Fig. 2 shows a number of differential AES spectra around

270 eV taken at different stages of MoC/Au surface formation. Spectrum (a) was obtained from a Mo_2C powder sample and is shown here as a reference of purely "carbidic" state of carbon. Spectra (b)–(e) represent the formation of a MoC/Au surface from a C_2H_4 + Mo overlayer at various temperatures. In all of the spectra, the triplet of positive peaks "B," which is considered a fingerprint of "carbidic" carbon [29,40], is clearly visible. This observation shows that carbide is the primary state of carbon at all stages of MoC formation.

More subtle changes in the carbon state can be inferred from the line shape of the negative peaks (features "A"). As the C_2H_4 + Mo overlayer is heated to 400 K, the carbon AES peak shape (Fig. 2d) becomes almost identical to that of Mo_2C (Fig. 2a). According to TPD studies, ethylene from the C_2H_4 + Mo overlayer completely decomposes (i.e., hydrogen desorption stops) at 400 K [27]. At this temperature, we would expect the surface to contain amorphous MoC_x clusters with all carbon in the carbide form. On annealing to 800 K, the carbon AES line shape changes and becomes similar to the line shape of near-graphitic carbon on a Ni(111) surface [39]. It has previously been shown that carbon becomes mobile in bulk Mo metal above 700 K [21]. We propose that the observed line shape change (d) → (e) in Fig. 2 is due to surface segregation of carbon on the MoC nanoparticles. Sputtering the top layer of the MoC/Au surface changes the carbon line shape back to a purely "carbidic" form (Fig. 2f), and annealing to 800 K returns the partially "graphitic" features (Fig. 2g). These observations can be interpreted as removal of surface "graphitic" carbon by sputtering and reprecipitation of carbon on annealing. Reprecipitation is possible because we do not expect MoC_x particles to reach thermodynamic equilibrium after annealing to 800 K. Such equilibrium in the bulk Mo sample was achieved only on annealing to 1150 K [21].

The precipitation of surface carbon is primarily a result of the high carbon content of the MoC particles prepared by the RLAD method using multiple layers of ethylene. As reported in our earlier studies, MoC/Au surfaces prepared by Mo deposition on a *single*, physisorbed layer of ethylene exhibited a smaller C/Mo ratio (1.0 ± 0.2) that *decreased* at higher annealing temperatures ($\geqslant$600 K). This affect was attributed to the diffusion of surface carbon into the bulk of the MoC particles, consistent with the behavior of other carburized Mo surfaces with carbon content below saturation (C/Mo $\leqslant 1.0$).

To summarize, we believe that thermal treatment of the MoC/Au surfaces can result in both preferential Au encapsulation of Mo-reactive sites and carbon precipitation on the surface, or in diffusion into the bulk, depending on initial carbon concentration. A more detailed analysis would require the use of experimental techniques that are only sensitive to the surface structure or composition, such as inelastic ion scattering.

4. Surface reactions

A typical TPD spectrum from a MoC/Au surface with slightly more than 1 ML of deuterated cyclohexene (c-C_6D_{10}) deposited at 85 K is shown by curves (a)–(c) in Fig. 3. Accord-

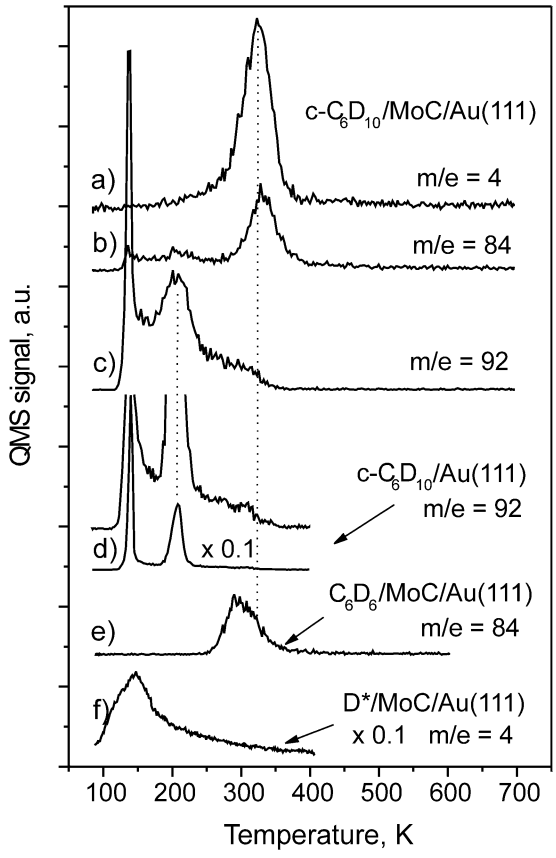

Fig. 3. (a)–(c) TPD spectrum from c-C_6D_{10}-exposed annealed MoC/Au(111) surface. Ionic signals corresponding to (a) D_2, (b) C_6D_6, and (c) intact c-C_6D_{10} are shown. TPD spectra (d)–(f) are shown for reference: (d) molecular desorption of c-C_6D_{10} from Au(111) surface (plotted in two scales); (e) molecular desorption of C_6D_6 from annealed MoC/Au(111) surface; (f) recombinative desorption of D_2 from annealed MoC/Au(111) surface.

ing to AES measurements, the surface contained 30% Mo and 33% C. The other spectra in Fig. 3, (d)–(f), are shown for reference; curve (d) is the desorption of cyclohexene from a clean Au(111) surface, curve (e) represents desorption of benzene (C_6D_6) from a MoC/Au surface, and curve (f) is desorption of D_2 from a MoC/Au surface exposed to D atoms. Intact c-C_6D_{10} desorption from the MoC/Au surface shows two peaks, at 140 and 210 K, and a wide shoulder between 140 and 320 K (see curve (c), Fig. 3). These two peaks are identified as multilayer and monolayer desorption of cyclohexene from gold areas of the MoC/Au surface, because the temperatures of these two peaks match the respective desorption temperatures from clean Au(111) (curve (d) in Fig. 3) [32]. The broader width of the monolayer desorption peak for the MoC/Au surface compared with the clean Au(111) surface probably arises from defects on the open Au areas resulting from presence of MoC particles.

Desorption of D_2 and benzene occur at 320 and 330 K, respectively (curves (a) and (b) in Fig. 3), and result from partial dehydrogenation of cyclohexene on the MoC/Au surfaces, that is,

$$\text{c-}C_6D_{10}(\text{ads}) \rightarrow C_6D_6(\text{g}) + 2D_2(\text{g}). \quad (1)$$

The simultaneous desorption of the two products suggests *reaction-limited* kinetics for this reaction. This conclusion is

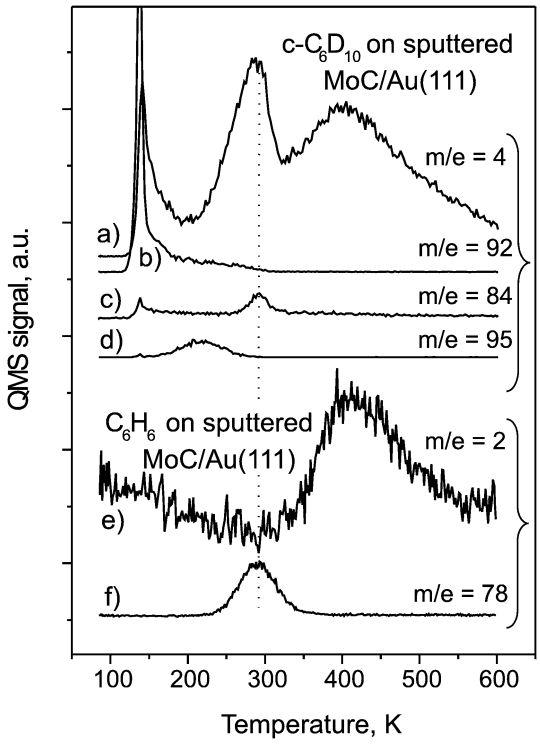

Fig. 4. TPD spectra from c-C_6D_{10}-exposed (a)–(d) and C_6H_6-exposed (e)–(f) sputtered MoC/Au(111) surface. Ionic signals corresponding to (a) D_2, (b) intact c-C_6D_{10}, (c) C_6D_6, (d) c-$C_6D_{11}H$, (e) H_2, and (f) C_6H_6 are shown.

consistent with the observation that both molecular desorption of benzene (curve (e), Fig. 3) and recombinative desorption of deuterium (curve (f), Fig. 3) occur at lower temperatures (<320 K).

The high temperature shoulder of the c-C_6D_{10} molecular desorption spectrum abruptly terminates very near the desorption temperatures for benzene and deuterium (310 K). This observation may seem to suggest a direct relationship between molecular and dissociative desorption processes on the MoC/Au surface; that is, the molecular desorption terminates exactly because the cyclohexene remaining on the surface is depleted through the dissociative desorption. In fact, the desorption of cyclohexene from Au(111) exhibits an almost identical desorption shoulder (full-scale curve (d) in Fig. 3). Thus the shoulder probably originates from surface defects present on both the Au(111) and the MoC/Au surfaces, such as steps on the Au(111) substrate.

As noted in the previous section, when the MoC nanoparticles are in an equilibrium state on the Au(111) surface, they are encapsulated by gold. To explore the influence of the encapsulation on reactivity, a number of TPD experiments were performed with a MoC/Au surface that was sputtered briefly at 200 K to remove about one atomic layer. Fig. 4, (a)–(d) shows TPD curves from a sputtered MoC/Au surface with slightly more than 1 ML of c-C_6D_{10} adsorbed at 85 K. The lower temperature peaks at 140 K for product masses at 92, 4, and 84 amu are ion fragments associated with multilayer desorption of molecular cyclohexene (electron-impact fragmentation in the mass spectrometer ionizer). Molecular deuterium desorbs in two wide overlapping peaks with maxima at 280 and 400 K (curve (a), Fig. 4). The only other desorption products observed were benzene and cyclohexane, with TPD peaks at 290 and 220 K, respectively (curves (c) and (d), Fig. 4). It should be mentioned that in the process of sputtering, the surface adsorbs significant amounts of hydrogen, probably from an increased H_2 background that results from the hot filament of the sputter gun. Adsorbed hydrogen manifests in H_2 and HD desorption peaks, nearly coincident with the first D_2 peak at 280 K, and in H/D isotope scrambling in desorbing benzene and cyclohexane. For example, the TPD curve for mass 83 amu (C_6D_5H) was identical to the TPD curve for mass 84 amu (C_6D_6) shown in curve (c) of Fig. 4, but at approximately half the intensity. Cyclohexane desorption at 220 K was also found in several H/D isotopic forms, including C_6D_{12}, $C_6D_{11}H$, and $C_6D_{10}H_2$, all of which exhibited the same TPD curve as the most abundant product, $C_6D_{11}H$, shown in curve (d) of Fig. 4.

The reaction/desorption processes resulting from cyclohexene on a sputtered MoC/Au surface can be interpreted by comparison with TPD spectra from an identical surface exposed to benzene (C_6H_6). These are shown in curves (e) and (f) in Fig. 4. To facilitate comparison, only the TPD data for nondeuterated benzene are shown, because hydrogen desorption is not isotopically scrambled into D_2 and HD components (although the TPD peaks for D_2/HD resulting from C_6D_6 reaction are essentially identical). It is seen that benzene desorbs from surfaces exposed to cyclohexene or benzene at identical temperatures of 290 K (curves (c) and (f)). The molecular hydrogen desorption peak from the benzene-exposed surface (curve (e)) is very similar in both temperature and area to the higher-temperature (400 K) deuterium desorption peak from the surface exposed to cyclohexene (curve (a)). The calculated areas of these two peaks differ by <20%. Note that curves (a) and (e) in Fig. 4 are plotted on the same scale, and the higher noise level in curve (a) is related only to high background levels of hydrogen ($m/e = 2$) in the vacuum chamber, as opposed to a virtually zero background of deuterium ($m/e = 4$). This comparison suggests that for cyclohexene on a sputtered MoC/Au surface, the benzene peak at 290 K and the higher temperature D_2 desorption peak at 400 K originate from adsorbed benzene intermediates. The lower-temperature deuterium TPD peak at 280 K can then be attributed to the recombination of adsorbed deuterium atoms produced in the process of cyclohexene conversion to the benzene intermediate. The overall process can be given as the following sequence of reactions:

$$\text{c-}C_6D_{10} \rightarrow C_6D_6(\text{ads}) + 4D(\text{ads}), \tag{2}$$

$$2D(\text{ads}) \rightarrow D_2(\text{g}) \quad \text{at 280 K}, \tag{3}$$

$$C_6D_6(\text{ads}) \rightarrow C_6D_6(\text{g}) \quad \text{at 290 K}, \tag{4}$$

and

$$C_6D_6(\text{ads}) \rightarrow 6C(\text{ads}) + 3D_2(\text{g}) \quad \text{at 400 K}. \tag{5}$$

The observation of cyclohexane desorption at 220 K is apparently also induced by adsorbed deuterium atoms produced in reaction (2),

$$\text{c-}C_6D_{10}(\text{ads}) + 2D(\text{ads}) \rightarrow \text{c-}C_6D_{12}(\text{g}) \quad \text{at 220 K}. \tag{6}$$

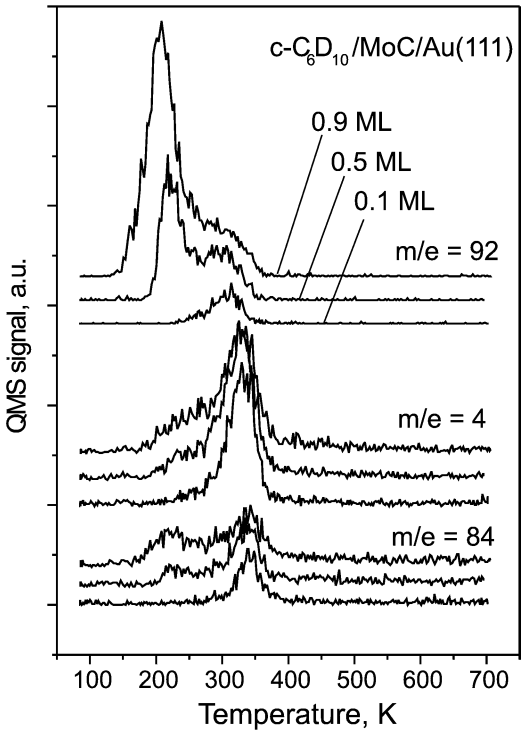

Fig. 5. TPD spectra from an annealed MoC/Au(111) surface dosed with varying coverages of c-C_6D_{10}.

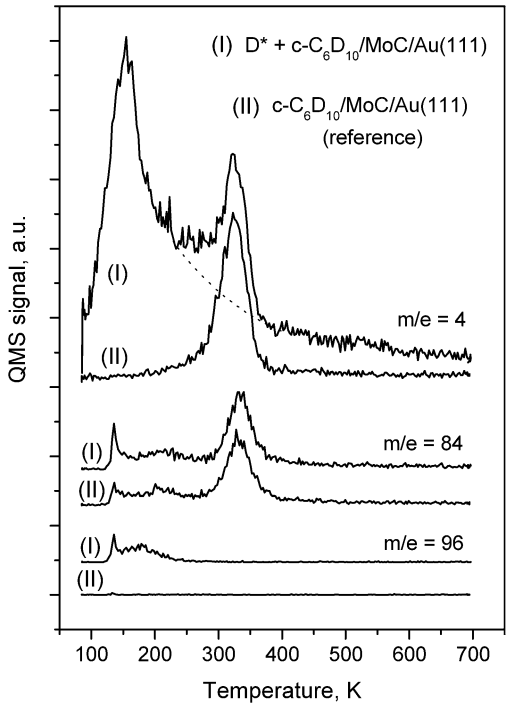

Fig. 6. TPD spectrum (I) from an annealed MoC/Au(111) surface exposed to atomic deuterium and then to c-C_6D_{10}. For comparison a TPD spectrum (II) from the same surface exposed only to c-C_6D_{10} is shown.

At the beginning of reaction (2), the surface is saturated with adsorbed cyclohexene (c-C_6D_{10}). A surface deuterium atom has a higher probability of association with cyclohexene (reaction (6)) than of association with another surface-bound deuterium (reaction (3)). As the surface population of cyclohexene is depleted in the temperature range 200–250 K by both its conversion to benzene and its desorption as cyclohexane, the probability of reaction (6) drops, and molecular deuterium desorption (reaction (3)) becomes the dominant process.

Results of TPD experiments (not shown) with cyclohexene dosed on bare Mo nanoparticles deposited on a Au(111) substrate were very similar to those shown in Fig. 4. The Mo/Au(111) surface was prepared by PVD of molybdenum on a Au(111) surface at 300 K. The temperature of the substrate during Mo deposition was chosen to minimize gold encapsulation of Mo while also minimizing the hydrogen content of the Mo nanoparticles [28]. Nonetheless, extensive H/D scrambling was observed with otherwise identical desorption products as seen for the sputtered MoC/Au surface exposed to c-C_6D_{10}. In a separate experiment, Au-encapsulated Mo nanoparticles on a Au(111) surface were found to be completely unreactive for cyclohexene.

Desorption experiments presented in Figs. 5 and 6 provide additional information on the nature of cyclohexene reactivity on the MoC/Au surface. Fig. 5 shows TPD results for varying cyclohexene (c-C_6D_{10}) coverages on the MoC/Au surface (Au-encapsulated). It can be seen that at coverages <0.1 ML, all cyclohexene is converted to benzene (C_6D_6) and D_2 (signals $m/e = 84$ and 4, respectively). At higher initial cyclohexene coverages, the intact cyclohexene desorption peak appears at 210 K, which we previously assigned to desorption from Au sites on the surface. In addition, the benzene and D_2 peaks do not grow with increasing initial cyclohexene coverage. The low-temperature shoulders that appear at higher coverages in signals $m/e = 4$ and 84 originate only from ionic fragmentation of molecular cyclohexene. This demonstrates that only a small fraction (<10%) of an adsorbed monolayer dissociates on the MoC/Au surface. Fig. 5 also clearly shows that cyclohexene is bound more strongly on MoC sites than on Au sites and that cyclohexene is sufficiently mobile at 200 K to selectively occupy all of the available sites on the MoC particles.

The experiment presented in Fig. 6 was meant to explore the formation of cyclohexane from cyclohexene on MoC/Au surfaces. Here the TPD spectra marked with (I) were obtained in an experiment where an annealed MoC/Au surface held at 85 K was exposed to atomic deuterium (∼1 L), then to 1 L of cyclohexene (c-C_6D_{10}). The spectra marked with (II) are used as a reference and were taken from the same surface exposed to 1 L cyclohexene, with no exposure to atomic deuterium. Fig. 6 shows that the presence of atomic hydrogen (deuterium) does not influence the amount of cyclohexene that undergoes dissociation on the surface, because the peaks at 320 K in spectra (I) and (II) have approximately the same area for both benzene ($m/e = 84$) and deuterium ($m/e = 4$). The D_2 desorption peak at 150 K from the surface exposed to D atoms has an identical temperature to, but only 1/2 the intensity of, a MoC/Au surface that is saturated with D atoms (curve (f) in Fig. 3). Desorption of cyclohexane ($m/e = 96$) was observed at 180 K from the surface exposed to atomic deuterium (I), but the intensity of the peak was about 1/3 that of the sputtered, cyclohexene-exposed MoC/Au surface (Fig. 4), despite an abundance of surface D atoms. This indicates that recombination of surface hy-

drogen (reaction (3)) is a more likely process than cyclohexane formation (reaction (6)). This is consistent with the argument given earlier that the formation of cyclohexane from a sputtered MoC/Au surface (Fig. 4) ceases when the cyclohexene coverage becomes low enough to hinder surface D (H) atom diffusion.

5. Quantitative analysis

Further details of the cyclohexene reactions on MoC/Au surfaces can be derived from a quantitative analysis of the TPD data, beginning with the sputtered MoC/Au surface shown in Fig. 4, (a)–(d). Using the integrated areas of the hydrogen (deuterium), benzene, cyclohexene, and cyclohexane peaks (along with the mass spectrometer relative sensitivity factors discussed in the Experimental section) it is possible to conduct a complete mass balance of the elements (carbon and deuterium) for the reactions on the surface. Interference of the surface hydrogen deposited during sputtering of the MoC/Au surface was also accounted for in these analyses. Defining the amount of cyclohexene left on the surface after desorption of the multilayer (i.e., a single layer) as 100%, we found that 35% of the cyclohexene completely decomposed to surface carbon and D_2 (reactions (2), (3), and (5)), 4% of the cyclohexene partially dehydrogenated to desorb as benzene (reactions (2) and (4)), 20% of the cyclohexene hydrogenated to form cyclohexane (reaction (6)), and 30% of the cyclohexene desorbed intact. Complete decomposition of cyclohexene should deposit carbon on the surface. Indeed, after the TPD experiment presented in Fig. 4, AES measurements showed a 12% increase in the surface carbon concentration.

According to our hypothesis, the first D_2 desorption peak at 280 K for cyclohexene reacting on the sputtered MoC/Au surface (denoted by I) is caused by partial dissociation of cyclohexene to benzene, and the second peak at 400 K (denoted by II) corresponds to complete dissociation of the benzene intermediate. If this hypothesis is correct, then the peak II/peak I area ratio should be equal to 3:2 (or 1.5). In calculating the areas of these two TPD peaks, we included both D_2 and HD desorption spectra, assuming equal sensitivity of the mass spectrometer at $m/e = 3$ and 4. To maintain the relative 3:2 stoichiometry of two desorption peaks, contributions from D_2 produced with benzene in reaction (1), and D_2 consumed by cyclohexane formation in reaction (6) were removed and added, respectively, to the area of peak I. These contributions were calculated from benzene and cyclohexane peak areas and their relative sensitivity factors. The peak II/peak I ratio in Fig. 4 was found to be equal to 1.3. Averaging over four independent experiments resulted in a value of 1.6 ± 0.3, which is consistent with the proposed reaction mechanism. The relatively large uncertainty of the calculated peak II/peak I ratio is related to the subjectivity in determination of the baseline and in the separation of the two TPD overlapping peaks.

Similar quantitative analysis of the TPD data presented in Fig. 3 shows that on the annealed MoC/Au surface, only 4% of a cyclohexene single layer partially dehydrogenates to form benzene at 320 K. The remaining 96% of the single layer desorbs as cyclohexene without chemical transformation. This result is consistent with the implications of the coverage dependence experiment shown in Fig. 5. The fraction of cyclohexene that partially dehydrogenates to benzene is surprisingly similar for the annealed (Au-encapsulated) and the sputtered MoC/Au surfaces. This result indicates that the increase in surface reactivity due to sputtering does not lead to an increase in active sites for selective dehydrogenation.

The values obtained from our calculations for the total amount of cyclohexene in single layers on the annealed and the sputtered MoC/Au surfaces differ by <20%. This is a reasonable result, because HREEL studies have shown that on both Au(111) and C/Mo(110) surfaces, cyclohexene molecules lie flat or nearly flat on the surface [17,32]. Thus we would expect the cyclohexene single layer coverage on a MoC/Au surface to be the same regardless of its atomic composition. The desorbing products from these two surfaces are very different, however (see Figs. 3 and 4), and these data were not used for determining the mass spectrometer sensitivity coefficients (obtained by independent calibration experiments). Therefore, the similarity of the single-layer coverages calculated for the sputtered and annealed MoC/Au surfaces is an independent confirmation of the quantitative analysis methodology used here.

In the analysis of the TPD data shown in Fig. 3, the molecular cyclohexene desorption peak at 200 K (spectrum (c)) is assigned to desorption from exposed Au(111) areas of the surface. By comparing the area of this peak to that of the monolayer desorption peak of cyclohexene from the clean Au(111) surface (spectrum (d) in Fig. 3), we estimate the fractional area of open Au(111) in our MoC/Au sample to be about 14%. This is consistent with elemental surface composition derived by AES: 30% Mo, 33% C, and 27% Au. However, the AES data cannot give a reliable estimate of the exposed Au(111) surface area, because the Au AES peak includes contributions from Au atoms below and on top (i.e., encapsulation) of the MoC particles.

Pertinent to the motivation of the present work is the determination of the selectivities of the MoC/Au surfaces for cyclohexene conversion to benzene versus complete decomposition. From the TPD data on the sputtered MoC/Au surfaces (see Fig. 4), molecular hydrogen (deuterium) resulting from the complete dehydrogenation of cyclohexene (reaction (5)) evolves at temperatures above 400 K. This is also true for the cyclohexene-covered Mo(110) and the (4×4)-C/Mo(110) surfaces, from which hydrogen desorbs with TPD peak maxima at 417 and 446 K, respectively [17]. In contrast, very little D_2 desorption is observed above 400 K from the annealed MoC/Au surface (Fig. 3, spectrum (a)). The small, nonzero D_2 desorption signal in this temperature range most likely originates from background gas in the chamber after the major D_2 desorption peak at 320 K, which is not completely removed because of limitations in pumping speed. Nonetheless, the integrated tail of the D_2 signal above 400 K was used to estimate the maximum possible extent of complete dissociation. A comparison of this integrated area to that of the D_2 desorption peak at 320 K, shows that no more than 5% of the benzene formed from cyclohexene dehydrogenation undergoes complete decomposition. AES could not give a more precise estimate of this value, because the maximum change in the surface carbon concentration due

to carbon deposition during a single TPD experiment would be <0.1%, far below the accuracy of our AES measurements.

6. Discussion

In general, the reactivity patterns of cyclohexene on the bare (sputtered) MoC nanoparticles on a Au(111) support are similar to those observed on Pt(111) and C/Mo(110) surfaces. A detailed TPD/XPS study on Pt(111) reported that about 37% of a cyclohexene single layer desorbs intact, 22% partially dehydrogenates with benzene formation, and the remaining 41% completely decomposes [18]. A TPD study has shown that cyclohexene on a C/Mo(110) surface completely decomposes with ∼33% selectivity and partially dehydrogenates to benzene with 67% selectivity [16]. According to the same study, 100% of the cyclohexene single layer decomposes completely on the Mo(110) surface [16].

Generally, the selectivity of a chemical process plays a more important role in catalysis than the overall reactivity. For an objective comparison of different surfaces, we consider only the cyclohexene that participates in dehydrogenation (either partial or complete) and use the fraction of this amount that partially dehydrogenates to benzene, γ, as a parameter reflecting the selectivity of the surface reaction. Accordingly, $\gamma = 0$ for the Mo(110) surface, which is typical for early transition metals. Formation of an interstitial carbide significantly passivates the surface (i.e., makes it more selective for the partial dehydrogenation): $\gamma = 0.7$ for C/Mo(110) surface. Oxygen modification of the C/Mo(110) surface at 900 K brings this parameter to $\gamma = 0.4$ [30]. From our data, $\gamma = 0.06$ for the sputtered MoC/Au surface, which is surprising given the higher C/Mo ratio of 1.1 observed by AES in our experiments compared with about 0.4 for the C/Mo(110) surface [30]. We explain the higher reactivity of the sputtered MoC/Au surface by its nanotexture. Molybdenum carbide forms compact clusters on the Au(111) surface of typical length scale of 5 nm [27]. As a result, MoC has many exposed low-coordination Mo sites that are responsible for more aggressive bond breaking compared with an atomically flat C/Mo(110) surface.

The formation of cyclohexane from cyclohexene has not been observed on any of the single-crystal surfaces. The presence of this unique reaction pathway on the sputtered MoC/Au surface is explained by significant local inhomogeneity of the surface. By this, we mean the coexistence of MoC and Au(111) areas in immediate proximity, as shown by scanning tunneling microscopy [27], and variation in local atomic composition of the MoC clusters, as implied in our discussion of carbon surface segregation (see Section 3). It can be envisioned that cyclohexene molecules dehydrogenate on more-reactive sites, with the abstracted hydrogen atom binding to a cyclohexene molecule located on a less-reactive site, ultimately leading to the desorption of cyclohexane. This process would not be likely on any atomically homogeneous surface, because the onset of dehydrogenation occurs at the same temperature for all of the adsorbed cyclohexene molecules. It is highly unlikely that a cyclohexene molecule can capture two hydrogen atoms produced somewhere else on the surface before it starts to lose its own hydrogens.

It has been shown that annealing of the as-prepared or sputtered MoC/Au surface to temperatures at or above 700 K results in Au encapsulation of the MoC nanoparticles. This Au encapsulation causes a radical change in the surface reactivity. Although the overall reactivity of the encapsulated MoC clusters is significantly lower than that of the bare clusters, the selectivity for the partial dissociation of cyclohexene is exceptionally high, with $\gamma > 0.95$. Apparently, the Au caps on the MoC clusters are not as dense the Au caps on Mo nanoparticles [28], because a separate experiment did not show any chemical interaction between cyclohexene and an annealed Mo/Au(111) surface. Gold appears to selectively block sites of higher reactivity on the surfaces of the MoC nanoparticles, making the surfaces still active for aliphatic C–H bond breaking but passive for C–C or olefinic C–H bond breaking (at the temperature of benzene desorption). A similar passivating effect of Au was observed in the case of hydrocarbon steam-reforming catalysis on supported Ni nanoparticles [42,43]. The addition of small amounts of Au to Ni significantly reduced carbon deposition rates on the surface of the catalyst; this effect was attributed to Au atoms blocking the reactive sites (edges and kinks) on the surface of the Ni nanoparticles [43]. In general, minimization of carbon deposition on a catalytic surface is an important goal in catalyst design because, under conditions of a continuous process, carbon buildup results in decreased reaction rates. From this point of view, the MoC/Au system demonstrates a clear advantage for the partial dehydrogenation of cyclohexene compared with both Pt(111) and C/Mo(110) surfaces.

In terms of the mechanism of cyclohexene dehydrogenation, the Au-encapsulated MoC/Au surface is very similar to a carbided Mo(110) surface. Benzene evolves from a cyclohexene exposed (4×4)-C/Mo(110) surface at 327 K—practically identical to the 330 K observed in our experiments [17]. It has also been concluded that the desorption of benzene from the (4×4)-C/Mo(110) surface is a *reaction-limited* process [17]. In the case of the Au-encapsulated MoC/Au surface, we can make a more specific conclusion from our TPD experiments: The rate-limiting step of reaction (1) must be the abstraction of the first hydrogen from the c-C_6D_{10} molecules, with the other three deuterium atoms breaking off in fast steps. If the step c-C_6D_{10}(ads) → c-C_6D_9(ads) + D(ads) occurred below 320 K, then we would observe a D_2 desorption peak at this lower temperature, because recombinative desorption of D atoms from this surface was observed at 150 K (see Fig. 3(f)). The surface reaction of cyclohexene on a Pt(111) surface gives an example of the opposite—*desorption limited*—kinetics [18]. Cyclohexene at submonolayer coverages dissociates into benzene and atomic hydrogen on the Pt(111) surface below 275 K, whereas molecular hydrogen and benzene desorb at 365 and 500 K, respectively [18].

7. Conclusion

Molybdenum carbide nanoparticles were prepared on a Au(111) support by depositing alternate layers of ethylene and

Mo on a gold surface at 85 K, followed by annealing to 700 K. Our estimate of C/Mo atomic ratio on the MoC_x/Au(111) surfaces is between 1.1:1 and 1.6:1, although some carbon may be in graphitic form on the surface. During the preparation of the molybdenum carbide nanoparticles, gold encapsulates the clusters during annealing. This encapsulation is not as extensive as that seen on metallic Mo clusters on the Au(111) surface. In contrast, the Au-encapsulated MoC nanoparticles are reactive for the partial dehydrogenation of cyclohexene at 320 K, in which benzene and molecular hydrogen are produced. The overall reactivity of the annealed surface is low, however, with only 4% of an adsorbed monolayer of cyclohexene undergoing dehydrogenation. In contrast, the selectivity of this reaction is surprisingly high, with $>95\%$ of the reacted cyclohexene converted to benzene. The MoC nanoparticles with Au encapsulation removed by sputtering showed a much higher reactivity; about $2/3$ of the cyclohexene monolayer reacted with the surface, but partial dehydrogenation to benzene was only a minor reaction pathway (4%). Most of the cyclohexene either decomposed completely to form surface carbon (35%) or was hydrogenated to cyclohexane (20%). The formation of cyclohexane from cyclohexene was not observed on any carburized Mo surface, which is attributed to local inhomogeneity of the MoC/Au(111) surface. On the other hand, the high selectivity of the reaction of cyclohexene with a Au-encapsulated MoC/Au(111) surface for the partial dehydrogenation to benzene is explained by Au atoms blocking high reactivity sites on the MoC clusters that are otherwise responsible for complete cyclohexene dissociation.

References

[1] J.G. Chen, Chem. Rev. 96 (1996) 1477;
R.L. Levy, M. Boudart, Science 181 (1973) 547;
S.T. Oyama, in: S.T. Oyama (Ed.), Chemistry of Transition Metal Carbides and Nitrides, Blackie Academic, Glasgow, 1996, p. 1, and references therein.

[2] S.T. Oyama, Catal. Today 15 (1992) 179.

[3] H.H. Hwu, J.G. Chen, Chem. Rev. 105 (2005) 185.

[4] F. Solymosi, A. Szechenyi, J. Catal. 223 (2004) 221.

[5] M.K. Neylon, S. Choi, H. Kwon, K.E. Curry, L.T. Thompson, Appl. Catal. A 183 (1999) 253.

[6] F. Solymosi, J. Cserenyi, A. Szoke, T. Bansagi, A. Oszko, J. Catal. 165 (1997) 150.

[7] D. Wang, J.H. Lunsford, M.P. Rosynek, J. Catal. 169 (1997) 347.

[8] K. Oshikawa, M. Nagai, S. Omi, J. Phys. Chem. B 105 (2001) 9124.

[9] J.B. Claridge, A.P.E. York, A.J. Brungs, C. Marquez-Alvarez, J. Sloan, S.C. Tsang, M.L.H. Green, J. Catal. 180 (1998) 85.

[10] T. Hyeon, M. Fang, K.S. Suslick, J. Am. Chem. Soc. 118 (1996) 5492.

[11] R. Kojima, K.-I. Aika, Appl. Catal. A 219 (2001) 141.

[12] S. Ramanathan, C.C. Yu, S.T. Oyama, J. Catal. 173 (1998) 10;
S. Ramanathan, S.T. Oyama, J. Phys. Chem. B 99 (1995) 16365.

[13] J.G. Choi, J.R. Brenner, L.T. Thompson, J. Catal. 108 (1995) 40;
D.J. Sajkowski, S.T. Oyama, Appl. Catal. A 134 (1996) 339.

[14] J. Patt, D.J. Moon, C. Phillips, L. Thompson, Catal. Lett. 65 (2000) 193;
J. Sehested, C.J.H. Jacobsen, S. Rokni, J.R. Rostrup-Nielsen, J. Catal. 201 (2001) 206;
A.R.S. Darujati, D.C. LaMont, W.J. Thompson, Appl. Catal. A 253 (2003) 397.

[15] P.M. Patterson, T.K. Das, B.H. Burton, Appl. Catal. A 251 (2003) 449.

[16] J.G. Chen, B. Fruhberger, Surf. Sci. 367 (1996) L102.

[17] J. Eng Jr., B.E. Bent, B. Fruhberger, J.G. Chen, Langmuir 14 (1998) 1301.

[18] J.A. Rodriguez, C.T. Campbell, J. Catal. 115 (1989) 500.

[19] H.W. Hugosson, O. Eriksson, L. Nordstrom, U. Jansson, L. Fast, A. Delin, J.M. Willis, B. Johansson, J. Appl. Phys. 86 (1999) 3758, and references therein.

[20] B. Fruhberger, J.G. Chen, Surf. Sci. 342 (1995) 38;
P. Reinke, P. Oelhafen, Surf. Sci. 468 (2000) 203.

[21] B. Fruhberger, J.G. Chen, J. Eng Jr., B.E. Bent, J. Vac. Sci. Technol. A 14 (1996) 1475.

[22] V.I. Bukhtiyarov, M.G. Slin'ko, Russian Chem. Rev. 70 (2001) 147, and references therein;
U. Heiz, W.-D. Schneider, in: K.-H. Meiwes-Broer (Ed.), Metal Clusters at Surfaces: Structure, Quantum Properties, Physical Chemistry, Springer, New York, 2000, p. 237, and references therein;
X. Lai, D.W. Goodman, J. Mol. Catal. A 162 (2000) 33, references therein.

[23] J.S. Lee, L. Vope, F.H. Ribeiro, M. Boudart, J. Catal. 112 (1988) 44;
L. Vope, M. Boudart, J. Solid State Chem. 59 (1985) 348.

[24] J.D. Oxley, M.M. Mdleleni, K.S. Suslick, Catal. Today 88 (2004) 139.

[25] T. Miyao, I. Shishikura, M. Matsuoka, M. Nagai, S.T. Oyama, Appl. Catal. A 165 (1997) 419, and references therein.

[26] J.S. Lee, K.H. Lee, J.Y. Lee, J. Chem. Phys. 96 (1992) 362;
L. Wang, L. Tao, M. Xie, J. Huang, Y. Xu, Catal. Lett. 21 (1993) 35.

[27] J.M. Horn, Z. Song, D.V. Potapenko, J. Hrbek, M.G. White, J. Phys. Chem. B 109 (2005) 44.

[28] D.V. Potapenko, J.M. Horn, R.J. Beuhler, Z. Song, M.G. White, Surf. Sci. 574 (2005) 244.

[29] C.L. Hedberg (Ed.), Handbook of Auger Electron Spectroscopy, Physical Electronics, Inc., Eden Prairie, MN, 1995.

[30] H.H. Hwu, M.B. Zellner, J.G. Chen, J. Catal. 229 (2005) 35.

[31] D. Syomin, J. Kim, B.E. Koel, G.B. Ellison, J. Phys. Chem. B 105 (2001) 8387.

[32] D. Syomin, B.E. Koel, Surf. Sci. 498 (2002) 61.

[33] R.F. Berg, Metrologia 42 (2005) 11.

[34] E. Vogel, E. Bich, R. Nimz, Physica A 139 (1986) 188;
E. Vogel, B. Holdt, T. Strehlow, Physica A 148 (1988) 46.

[35] Z. Dohnalek, J. Kim, 2004, unpublished data.

[36] D. Ugarte, Chem. Phys. Lett. 209 (1993) 99.

[37] E. Sutter, 2005, unpublished data.

[38] T.Y. Velikanova, V.Z. Kublii, B.V. Khaenko, Sov. Powder Metall. Metal Ceram. 27 (1988) 891.

[39] A. Amoddeo, L.S. Caputi, E. Colavita, J. Electron Spectrosc. Relat. Phenom. 62 (1993) 263.

[40] J. Brillo, H. Kuhlenbeck, H.-J. Freund, Surf. Sci. 409 (1998) 199.

[41] K. Robbie, S.T. Jemander, N. Lin, C. Hallin, R. Erlandsson, G.V. Hansson, L.D. Madsen, Phys. Rev. B 64 (2001) 155401.

[42] F. Besenbacher, I. Choredorff, B.S. Clausen, B. Hammer, A.M. Molenbroek, I. Stensgaard, Science 279 (1998) 1913.

[43] A.M. Molenbroek, J.K. Norskov, B.S. Clausen, J. Phys. Chem. B 105 (2001) 5450.